

---

# SYNTHETIC IMAGE DETECTION WITH CLIP: UNDERSTANDING AND ASSESSING PREDICTIVE CUES

---

**Marco Willi**

Institute for Data Science I4DS  
 University of Applied Sciences FHNW  
 Brugg-Windisch AG, Switzerland  
 marco.willi@fhnw.ch

**Melanie Mathys**

Institute for Data Science I4DS  
 University of Applied Sciences FHNW  
 Brugg-Windisch AG, Switzerland  
 melanie.mathys@fhnw.ch

**Michael Graber**

Institute for Data Science I4DS  
 University of Applied Sciences FHNW  
 Brugg-Windisch AG, Switzerland  
 michael.graber@fhnw.ch

February 10, 2026

## ABSTRACT

Recent generative models produce near-photorealistic images, challenging the trustworthiness of photographs. Synthetic image detection (SID) has thus become an important area of research. Prior work has highlighted how synthetic images differ from real photographs—unfortunately, SID methods often struggle to generalize to novel generative models and often perform poorly in practical settings. CLIP, a foundational vision-language model which yields semantically rich image-text embeddings, shows strong accuracy and generalization for SID. Yet, the underlying relevant cues embedded in CLIP-features remain unknown. It is unclear, whether CLIP-based detectors simply detect strong visual artifacts or exploit subtle semantic biases, both of which would render them useless in practical settings or on generative models of high quality. We introduce *SynthCLIC*, a paired dataset of real photographs and high-quality synthetic counterparts from recent diffusion models, designed to reduce semantic bias in SID. Using an interpretable linear head with de-correlated activations and a text-grounded concept-model, we analyze what CLIP-based detectors learn. CLIP-based linear detectors reach 0.96 mAP on a GAN-based benchmark but only 0.92 on our high-quality diffusion dataset *SynthCLIC*, and generalization across generator families drops to as low as 0.37 mAP. We find that the detectors primarily rely on high-level photographic attributes (e.g., minimalist style, lens flare, or depth layering), rather than overt generator-specific artifacts. CLIP-based detectors perform well overall but generalize unevenly across diverse generative architectures. This highlights the need for continual model updates and broader training exposure, while reinforcing CLIP-based approaches as a strong foundation for more universal, robust SID.

## 1 Introduction

The rapid advancement in the quality of image generative models [45, 42, 21, 28, 33] has made it increasingly difficult to distinguish between real and synthetic photographs [34, 5, 38]. This enables nefarious actors to create convincing material to deceive and manipulate their targets, for example in disinformation campaigns or cyber influence operations [7, 10, 22]. Consequently, there is a growing body of research focused on detecting synthetic imagery [36, 50, 15, 48] to mitigate such risks.

Synthetic image detection (SID) methods often exploit model specific *fingerprints* [36]—subtle traces originating from the generative process—to identify synthetic images. Supervised learning algorithms can be trained to recognize these fingerprints with high accuracy [50]. Such approaches, however, suffer from two major limitations: (i) their accuracy

is often tightly coupled to the specific generative model used for model training [57], and ii) they are vulnerable to adversarial attacks that remove or obscure these low-level cues [4]. Consequently, SID methods require constant re-training and have unknown effectiveness in open-set conditions where test-time generative models might differ from those seen during training [20] (referred to as generalization).

A recent line of work investigates the utility of foundational vision models—trained with self-supervised objectives on internet-scale datasets—for synthetic image detection. Particularly, the CLIP model [43] has been a focus of intensive research [39, 8, 27, 30, 23, 32, 14, 17]. CLIP is trained on large-scale datasets of image-text pairs with the objective of maximizing similarity between matching pairs in a joint text-vision embedding space. The semantic richness of CLIP’s visual encoder, combined with its robustness to distribution shifts [43], makes it a promising candidate for detecting synthetic images. Unlike fingerprint-based methods, CLIP-based detectors may leverage high-level semantic inconsistencies [14]—potentially arising from object context, composition, or fine-grained detail. This shift in detection strategy suggests that CLIP may offer greater robustness to image post-processing, adversarial perturbations, and better generalization accuracy.

This raises a fundamental question: *If CLIP-based detectors do not rely on low-level fingerprints, what features do they actually use to distinguish real from synthetic images? Furthermore, how effective are CLIP-based methods considering generative models continue to improve in fidelity and diversity?*

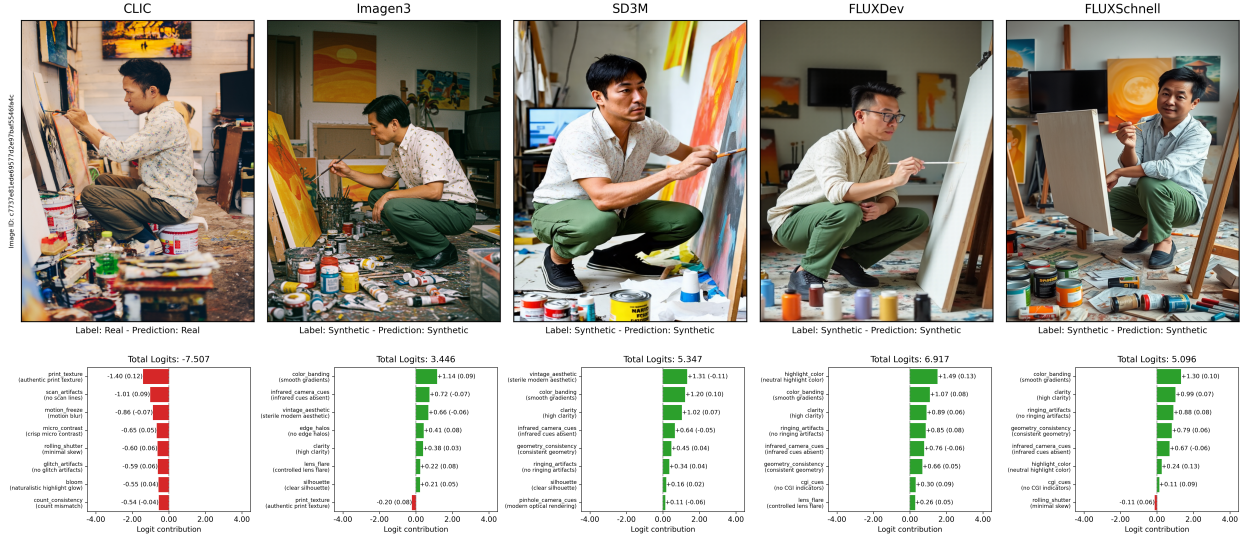


**Figure 1:** Synthetic images—even those generated by recent, high-quality generative models—differ from real photographs in subtle aspects. The figure shows a real image (left) and four paired synthetic variants from the SynthCLIC dataset. Shown are the most relevant terms (absolute logit contribution) of a concept model for the different images. Green bars (positive logit contribution) indicate concepts that contribute to the attribution of the synthetic class, while red bars (negative logit contribution) contribute to the real class. Shown are concept-individual contributions to the class logits and cosine similarities between concept and image embedding (in parentheses). Best viewed zoomed in. Photo credit Adli Wahid / Unsplash.

Specifically, we address the following questions:

- Q1 How well do CLIP-based detectors scale from GAN-based to modern diffusion-based synthetic images in realistic, paired datasets?
- Q2 Can we explain CLIP-based classifications using i) linear heads based on de-correlated image representations and / or ii) human-interpretable concepts based on vocabularies tailored to SID?
- Q3 Which visual and photographic attributes in CLIP representations are actually used to distinguish real from synthetic?

We seek to answer these questions by systematically analyzing the behavior and capabilities of CLIP-based synthetic image detectors. We leverage CLIP’s cross-modal nature to probe its visual representations with textual descriptions, offering an interpretable window into what drives its predictions. Additionally, we evaluate CLIP-based detectors across datasets of varying generative quality to understand their performance boundaries and failure modes.

Our contributions are threefold:

1. To address Q1 we construct a novel dataset, *SynthCLIC*, consisting of high-resolution real photographs from the *CLIC* dataset. For each photograph we generate synthetic counterparts with recent generative models, conditioned on captions generated from visual language models.
2. To address Q2 we train and evaluate CLIP-based classifiers using orthogonality constraints and concept-based classifiers with tailored vocabularies.
3. We address Q3 by analyzing the image features leveraged by CLIP on datasets of different quality and photo-realism and observe a shift in feature importance between GAN-based and modern high-quality diffusion-based models.

## 2 Previous Work

### 2.1 Generative Modeling

Generative models learn the distribution of a dataset and enable sampling of new data points. Often, such models allow for conditional generation, for example, to condition on class labels or textual descriptions. Recent advances in generative modeling have enabled near photo-realistic creation of images. There are different model types, such as generative adversarial networks (GANs) [25], variational autoencoders (VAEs) [31], normalizing flows [18], autoregressive models [56, 40], and diffusion models (DMs) [26]. In particular, DMs have demonstrated impressive generative quality, such as the stable diffusion family of models [45, 42, 21]. Furthermore, there are commercial providers which offer access to proprietary (and sometimes open-source) models, such as Midjourney [37], Google’s Imagen3 [28], Black Forest’s Flux models [2], Adobe’s Firefly models [1], or OpenAI’s GPT-Image [29]. The most recent advances include multi-modal large language models which can be used to generate images and text consistently and in conditional sequences [54, 58], including image captioning.

### 2.2 Synthetic Image Detection (SID)

Generative models leave invisible traces—also referred to as *artificial fingerprints*—in generated images, which are tied to the generative process [36]. These fingerprints can be visualized by calculating the average frequency spectra of images from generative models [57, 36]. This has been demonstrated for different models and architecture types, including diffusion models [11]. A common approach to SID is to model it as a binary classification task using a dataset of real and synthetic images. Several works [50, 12, 44, 47, 51, 52, 53], demonstrated that this approach can achieve high accuracy. Models trained for SID tend to generalize poorly to synthetic images from models not seen during model training [13]. Generalization improves with aggressive data augmentation during model training, such as post-processing operations like image compression [50]. However, models do not generalize across substantial architectural changes, e.g., from GANs to Diffusion models [20]. Additionally, SID models remain vulnerable to adversarial attacks, as shown in both white-box and black-box scenarios [4, 59]. Furthermore, optimal detection thresholds vary for accurate detection of synthetic images from different generative models, making it necessary to calibrate model predictions when doing inference on synthetic images from novel sources.

### 2.3 CLIP-based Synthetic Image Detection

A growing body of work demonstrates that CLIP’s image representations are remarkably effective for SID [39, 8, 27, 30, 23, 32, 14, 17]. A common paradigm is to extract features using CLIP’s frozen image encoder and train a lightweight classifier—typically logistic regression or a linear SVM—on top of those features. Across studies, CLIP-based representations consistently outperform features from supervised models in both accuracy and generalization.

A central insight from this line of work is the effectiveness of contrastive pre-training combined with the vision transformer (ViT) architecture [19], as opposed to CNN-based backbones. CLIP-ViT embeddings not only outperform supervised ImageNet features for SID but also naturally separate real from synthetic images in 2D t-SNE projections, even without fine-tuning [39]. These findings demonstrate the inherent discriminative capacity of CLIP representations for SID.

Another important thread investigates the layer-wise utility of CLIP representations. While most studies use (near) final image embeddings, several works show that intermediate layers contain richer low-level cues crucial for detecting artifacts and visual fingerprints. Fusing intermediate and final-layer features with a learnable module yields substantial gains [32]; intermediate features also outperform early or late layers in open-set and out-of-distribution scenarios, particularly with limited training data [8].

A third theme is robustness and data efficiency. CLIP-based detectors generalize to unseen generative models and remain stable under perturbations such as compression and resizing; they achieve strong performance with as few as 10 training examples, with diminishing returns beyond roughly 10,000 image pairs. Mitigating semantic biases via paired training—generating a synthetic counterpart from a real image’s caption—further improves reliability [14].

Finally, joint adaptation of CLIP’s visual and textual components has been explored. Comparisons of linear probing, fine-tuning, prompt tuning, and adapters identify prompt tuning as most effective in many settings; leveraging the text encoder through systematic input adaptation can further enhance SID, though results vary across datasets [30].

## 2.4 Why are CLIP-based Detectors Effective?

CLIP models are pre-trained on massive datasets of image-text pairs—400 million in the original release [43], and over 2 billion in recent variants [6, 46]. This scale and diversity enables CLIP to learn rich, generalizable visual features by aligning images with textual descriptions. Models trained from scratch in a supervised setting may focus on the (easy) task of detecting generative fingerprints and thus ignore potential features related to real photographs [39]. This behavior could lead to poor generalization: in the absence of model-specific fingerprints everything gets classified as real. Models not explicitly trained for SID might provide a richer, and better suited feature-space [39].

[14] showed that CLIP-based detectors retain high performance under image manipulations such as resizing and compression, which often degrade the subtle traces exploited by conventional detectors. They found that supervised models (CNNs trained from scratch) fail when (i) synthetic images are resized to suppress high-frequency artifacts, or (ii) real images are modified using an autoencoder to embed artificial fingerprints. In contrast, CLIP-based detectors remain effective, suggesting their decisions are based on features beyond low-level image statistics.

[17] examined the adversarial robustness of CLIP- and CNN-based SID models. Their Fourier-domain analysis revealed that adversarial perturbations targeting CLIP tend to affect a wider frequency range, particularly lower components, than those targeting CNNs. Consistently, they observed that low-pass filtering disproportionately harms CNN-based detectors. Overall, this is indicative of larger image structures being involved in CLIP-based SID approaches. Although CLIP is not inherently more robust to adversarial attacks, adversarial examples rarely transfer between CLIP and CNN architectures, underscoring fundamental differences in the features they exploit.

## 2.5 Interpreting CLIP-based Models

CLIP embeds images and text in a shared space, enabling zero-shot classification and geometric analyses (e.g., linear directions aligned with textual prompts) [43].

For SID, [23] align linear-probe weights with text embeddings, prune redundant features, and inspect attention heads. This reveals blur-related cues and dataset artifacts as being relevant features for CLIP-based SID; tokens like “blurry”/“blur” correlate with specific image generators, while “deeplearning”/“generative” associate with GANs—likely reflecting captions in CLIP’s pretraining data. Experiments span GAN-based datasets and paired images from several text-conditional diffusion models.

Complementary research, unrelated to SID, reports head-level specialization in ViT-based CLIP and introduces *TextSpan*, which constructs a semantic basis for each attention head by matching activations to text embeddings [24]. A related but distinct line of work, concept discovery models [41], links a set of human-interpretable concepts to images by introducing per-example binary concept-selection latents (with a Bernoulli prior) and learning them end-to-end by maximizing an ELBO.

## 2.6 Relation to prior CLIP-based SID

Prior work has demonstrated the effectiveness of CLIP features for SID, typically by training linear classifiers or shallow heads on top of CLIP’s final image embedding and evaluating on specific benchmarks and generator families. In contrast, we (i) evaluate CLIP-based SID across three datasets including a new paired dataset (*SynthCLIC*) with high-quality diffusion-based images derived from CLIC, (ii) use CLIP’s last hidden state with a low-dimensional orthogonal linear head that is explicitly designed for interpretability, and (iii) adapt sparse linear concept discovery models to CLIP-based SID using photography-oriented vocabularies. This allows us not only to quantify detection performance but also to investigate which visual and photographic attributes CLIP relies on when deciding whether an image is real or synthetic.



**Figure 2:** Examples from the *SynthBuster+* dataset. Different paired images are shown in each row. Each column depicts a different image source, starting with real photographs from the RAISE-1K dataset [16], followed by synthetic images from the *Synthbuster* dataset [3] and images added by us: *Imagen 3* [28], *FluxDev* and *FluxSchnell* [2], and *Stable Diffusion 3 Medium* [21].

### 3 Method

#### 3.1 Image Data

We use three different datasets for our experiments. The first, *CNNSpot*, was introduced by [50] and is used in many subsequent works for SID, including CLIP-based approaches [39]. The dataset consists of a training set based on synthetic images generated solely by the ProGAN method, which was trained to generate 20 different classes from the LSUN [55] dataset. The test set of *CNNSpot* is more diverse and includes images from 11 different generative models, mostly based on GANs. For efficiency reasons and because previous work (e.g. [14]) demonstrated low sensitivity to the number of training images, we only use 1k training images, instead of the full dataset with 720k images. Example images can be found in Appendix A.1.

Additionally, we use the *SynthBuster* dataset [3] which is based on real photographs (RAISE-1K) [16] and corresponding, paired synthetic images which were generated with text-conditional generative models to match the content of the real photographs as closely as possible. The dataset includes images from nine different generative latent diffusion models. We augment the dataset with synthetic images from more recent models to reflect the current generative quality and name the dataset *SynthBuster+*. Qualitative examples illustrating the dataset are provided in Figure 2.

We observe that the real photographs used in *SynthBuster* are not quite recent and lack diversity, with a strong bias toward outdoor and street scenes. Moreover, many real images appear overly bright and of relatively low photographic quality. To mitigate the risk that detectors exploit these biases, we construct an additional dataset, which we call *SynthCLIC*. As a basis, we use real photographs from the 6th Challenge on Learned Image Compression (CLIC)<sup>1</sup>. These images include both professionally captured photographs and images taken with mobile phones. We then use the same generative models as those used to extend the *SynthBuster* dataset to generate corresponding synthetic images. Figure 3 shows some example images.

We create images using *Imagen 3* [28], *FluxDev* and *FluxSchnell* [2], and *Stable Diffusion 3 Medium* [21] (see Appendix A.2 for exact model versions used). We aim at preserving the aspect ratio of each corresponding real image. We condition the generation process on descriptions derived from *Gemini* [9], a commercial visual large language model. Table 1 provides an overview of the datasets, including the split sizes used for model training, validation (a subset of the training set, used for early stopping), and testing. In paired datasets any real image and its synthetic variants are assigned to the same split.

To characterize and compare the synthetic images used in our experiments, and in particular to rule out trivial differences or biases, we employed a method from Image Quality Assessment (IQA). Such methods aim to quantify the *look* and *feel* of images from a human perspective. We used CLIP-IQA [49], a CLIP-based approach, to score several photographic attributes. The resulting score distributions show limited overlap for some attributes, such as *quality*, *beautiful*, *noisiness*, and *sharpness* (see Appendix B.1), suggesting that CLIP-based detectors can, to some extent,

<sup>1</sup><http://www.compression.cc/>

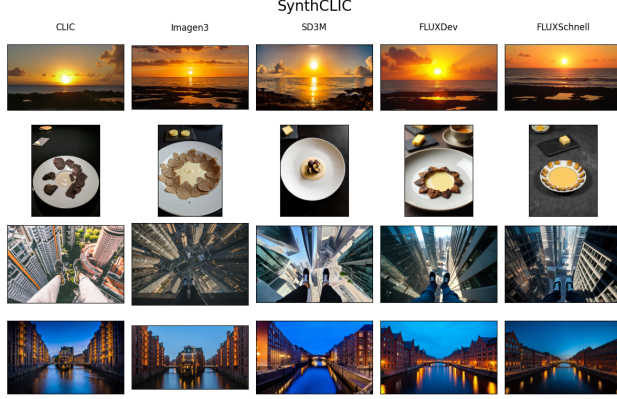


**Figure 3:** Examples from the *SynthCLIC* dataset. Different paired images are shown in each row. Each column depicts a different image source, starting with real photographs from the *CLIC* dataset, followed by synthetic images generated with *Imagen3* [28], *FluxDev* and *FluxSchnell* [2], and *Stable Diffusion 3 Medium* [21].

	Train		Validation		Test	
	Real	Synthetic	Real	Synthetic	Real	Synthetic
CNNSpot	1000	1000	1000	1000	54970	52980
SynthBuster+	640	8319	160	2080	200	2600
SynthCLIC	1633	6532	102	408	428	1712

**Table 1:** Datasets and the number of real and synthetic images, including split sizes, used in subsequent experiments. For models trained all datasets (combined) the size is the sum over the individual datasets.

exploit these cues to distinguish real from synthetic images. At the same time, visual inspection of paired images reveals strong semantic similarity between real and synthetic versions (Figures 2 and 3).

### 3.2 Evaluation settings

We consider three evaluation settings. (i) In-dataset (closed-set) detection: train and test on the same dataset, which measures performance when the detector is matched to both the real-image distribution and the set of generators used in that dataset. (ii) Cross-dataset generalization with overlapping generators: train on one diffusion-based dataset (*SynthBuster+* or *SynthCLIC*) and evaluate on the other. In this case, many underlying diffusion models overlap, but the real-image distributions, prompts, and generation pipelines differ, so the task mainly probes robustness to content and distribution shift rather than to completely unseen generators. (iii) Cross-family generalization: train on *CNNSpot* (GAN-based) and evaluate on the diffusion-based datasets, and vice versa, which combines both a change in real-image distribution and a shift in generator family.

### 3.3 CLIP Classifier

We use a pre-trained CLIP model, the ViT-L/14-336 variant<sup>2</sup>, based on the vision transformer architecture [19]. Let  $L$  denote the total number of transformer layers in the vision encoder. We use the hidden-state activations  $\mathbf{a}^l \in \mathbb{R}^d$  of the [CLS] token from a specific layer  $l$ , where in our experiments  $l = L$ , i.e., the final transformer layer, and  $d = 1024$ .

CLIP includes a learned projection head that maps the final vision features to a  $p$ -dimensional cross-modal embedding space shared with the text encoder. We discard this projection head and instead add two learnable linear layers to project the [CLS] token hidden state to lower dimensional spaces  $\mathbf{a}^{l+1} = \mathbf{a}^l \mathbf{W}_{\mathbf{L}1}$  and  $\mathbf{a}^{l+2} = \mathbf{a}^{l+1} \mathbf{W}_{\mathbf{L}2}$ , where  $\mathbf{W}_{\mathbf{L}1} \in \mathbb{R}^{d \times k}$  and  $\mathbf{W}_{\mathbf{L}2} \in \mathbb{R}^{k \times 1}$ . Let  $\bar{\mathbf{A}}^{l+1} \in \mathbb{R}^{n \times k}$  denote the row-wise  $\ell_2$ -normalize mini-batch activations of the first projection layer  $\mathbf{A}^{l+1}$ . The loss in Equation 1 combines binary cross-entropy (BCE) with an orthogonality constraint on  $\bar{\mathbf{A}}^{l+1}$ :

$$\mathcal{L}(\mathbf{y}, \hat{\mathbf{y}}) = \mathbb{E}_{\mathbf{x}, \mathbf{y}} [\text{BCE}(\hat{\mathbf{y}}, \mathbf{y})] + \lambda \left\| \mathbf{I} - (\bar{\mathbf{A}}^{l+1})^T \bar{\mathbf{A}}^{l+1} \right\|_F^2 \quad (1)$$

<sup>2</sup><https://huggingface.co/openai/clip-vit-large-patch14-336>

This encourages a low-dimensional representation with de-correlated features for improved interpretability. We set  $\lambda = 0.33$  for all experiments. Label smoothing, weight decay, data augmentation, and early stopping are also applied for regularization.

The CLIP vision encoder is kept frozen during training. We use different datasets as described in Section 3.1. The approach is very similar to other works. The study in [39] used a single linear layer, functionally equivalent to our design since we do not use a non-linearity, but applied it to the final  $p$ -dimensional cross-modal image embeddings. In contrast, we operate directly on the hidden-state activations from layer  $l = L$ . [14] used the same vision features as in our approach, but replaced the linear classifier with an SVM. Some training splits are substantially imbalanced (Table 1); we do not apply class re-weighting or re-sampling, and therefore emphasize threshold-independent metrics such as mAP. See Appendix A.3 for more details.

### 3.4 Assessing the Importance of Learned Representations

We assess the importance of each column vector  $[\mathbf{w}_0, \dots, \mathbf{w}_{k-1}]$  in  $\mathbf{W}_{\mathbf{L}1}$  by calculating their contribution to the class logits. For a given input image  $\mathbf{x}^{(i)}$ , indexed by  $i$ , we calculate activations  $\mathbf{A}_{\mathbf{L}1i} \in \mathbb{R}^{1 \times k}$ , logits  $z_i = \mathbf{A}_{\mathbf{L}1i} \mathbf{W}_{\mathbf{L}2}$ , and per-column contributions  $\mathbf{c}_i = \mathbf{A}_{\mathbf{L}1i} \odot \mathbf{W}_{\mathbf{L}2} \in \mathbb{R}^{1 \times k}$ . Define index sets  $\mathcal{I}_1 = \{i : y_i = 1\}$  (synthetic) and  $\mathcal{I}_0 = \{i : y_i = 0\}$  (real). We compute class-wise mean contribution vectors

$$\boldsymbol{\mu}_1 = \frac{1}{|\mathcal{I}_1|} \sum_{i \in \mathcal{I}_1} \mathbf{c}_i, \quad \boldsymbol{\mu}_0 = \frac{1}{|\mathcal{I}_0|} \sum_{i \in \mathcal{I}_0} \mathbf{c}_i, \quad (2)$$

and their difference  $\Delta\boldsymbol{\mu} = \boldsymbol{\mu}_1 - \boldsymbol{\mu}_0 \in \mathbb{R}^k$ . The  $j$ -th entry of  $\Delta\boldsymbol{\mu}$  quantifies how column  $j$  shifts evidence toward class 1 (synthetic) vs. class 0 (real). A positive value indicates higher average contribution to class 1; a negative value indicates higher average contribution to class 0.

### 3.5 Interpreting Learned Representations

To interpret learned directions (the columns of  $\mathbf{W}_{\mathbf{L}1}$ ) we compare them to vocabulary terms  $C$ . We use CLIP’s text encoder to embed vocabulary terms to CLIP’s  $p$ -dimensional cross-modal embedding space and obtain  $\mathbf{C} \in \mathbb{R}^{n \times p}$  with a vocabulary of  $n$  terms. We project  $\mathbf{W}_{\mathbf{L}1}$  using CLIP’s image projection head to obtain learned representations in  $\mathbb{R}^{p \times k}$  and compute cosine similarities between these representations and the vocabulary embeddings  $C$ . Analysing the similarities enables interpretation of the learned representations. For the antonym vocabulary  $C_{\text{antonyms}}$  (see Section 3.7), we rank attributes by the magnitude of signed cosine similarity to identify the most strongly aligned axes, and we report the sign to indicate whether the learned direction corresponds to the positive or negative pole.

### 3.6 Concept Modeling

Our concept model follows the Sparse Linear Concept Discovery Models (CDMs) [41], which use CLIP image–text similarities and a variational Bernoulli prior to obtain sparse linear concept activations. We adopt this framework for binary SID on *CNNSpot*, *SynthBuster+*, and *SynthCLIC* with photography-oriented vocabularies tailored to real vs synthetic cues.

Let  $\mathbf{C} \in \mathbb{R}^{n \times p}$  be the row-normalized concept embeddings with  $n$  terms,  $\mathbf{I} \in \mathbb{R}^{m \times p}$  the row-normalized image embeddings for  $m$  samples, and  $\mathbf{S} = \mathbf{I}\mathbf{C}^T \in \mathbb{R}^{m \times n}$  their cosine similarities. Following [41], we use a binary relevance mask  $\mathbf{Z} \in \{0, 1\}^{m \times n}$  to flexibly select concepts per sample.  $W_c \in \mathbb{R}^{n \times 1}$  is a learnable weight that selects task-relevant concepts. The class logits  $\mathbf{a} \in \mathbb{R}^{m \times 1}$  are thus:

$$\mathbf{a} = (\mathbf{S} \odot \mathbf{Z}) W_c \quad (3)$$

During training, we treat the relevance mask  $\mathbf{Z}$  as a latent variable and infer it with a factorized Bernoulli variational posterior. For each sample  $i$  (row  $\mathbf{z}_i$  of  $\mathbf{Z}$ ), we set

$$q(\mathbf{z}_i) = \text{Bernoulli}(\sigma(\mathbf{I}_i \mathbf{W}_s^\top)), \quad (4)$$

$$p(\mathbf{z}_i) = \text{Bernoulli}(\alpha), \quad (5)$$

where  $\mathbf{W}_s \in \mathbb{R}^{n \times p}$  is a learned projection from image-embedding space to per-concept logits (with  $p$  the embedding dimension),  $\sigma(\cdot)$  is applied element-wise, and the scalar  $\alpha$  is fixed across concepts to encourage sparsity. We optimize the negative ELBO:

$$\mathcal{L}(\mathbf{y}, \hat{\mathbf{y}}) = \mathbb{E}_{\mathbf{x}, \mathbf{y}} [\text{BCE}(\sigma(\mathbf{a}), \mathbf{y}) + \beta \text{KL}(q(\mathbf{z}) || p(\mathbf{z}))] \quad (6)$$

where BCE is the binary cross-entropy for SID, KL regularizes the inferred masks toward the sparse prior, and  $\beta$  controls the sparsity–accuracy trade-off.

### 3.7 Vocabularies

For the concept models (Section 3.6) and for interpreting the CLIP classifier (Section 3.5), we use two vocabularies embedded in CLIP’s  $p$ -dimensional space: (i) *TextSpan* (3,498 descriptions,  $C_{\text{textspan}}$ ) from [24]; and (ii) a photography-focused antonym vocabulary (168 attributes,  $C_{\text{antonyms}}$ ) consisting of paired attribute descriptors (e.g., *sharp detail*  $\leftrightarrow$  *blurry detail*) with corresponding prompt templates. For each attribute, we embed the positive and negative prompts with CLIP and form a single attribute direction by subtracting the normalized negative embedding from the normalized positive embedding, followed by  $\ell_2$  normalization; this yields one embedding vector per attribute name. We generated a long list of candidate attributes and antonym pairs using ChatGPT with a prompt that requests photographic and perceptual cues (e.g., color, lens effects, technique) while discouraging object semantics, and that outputs standardized positive/negative prompts. See Table 2 for examples (prompts not shown, only attributes).

Attribute	Positive	Negative	Category
saturation	balanced saturation	oversaturation	color
vibrance	high vibrance	muted palette	color
vignetting	subtle vignetting	heavy vignetting	lense
glitch artifacts	no glitch artifacts	glitch artifacts	others

**Table 2:** Example vocabulary antonym pairs used for constructing  $C_{\text{antonyms}}$ . Prompts are generated for each of the positive and negative aspects, embedded into CLIP’s feature space,  $\ell_2$ -normalized, subtracted from each other (positive - negative), and again  $\ell_2$ -normalized. This yields a single direction for each attribute.

## 4 Experiments and Results

In the following section we present different experiments and their results. Where applicable we evaluate model performance using classification accuracy (ACC), average precision (AP), and mean AP (mAP) if calculated across several datasets, following other studies in the field of SID [39, 14, 30, 50]. If not stated otherwise, we use a threshold of 0.5 to assign images to the positive class for accuracy calculation. Often we show results for models trained on *CNNSpot* and *SynthCLIC* to contrast results on (mainly) GAN-generated lower-quality synthetic images with high-quality diffusion model-based images.

### 4.1 CLIP Classifier

We trained four different models following the approach described in Section 3.3, each with a different training set. The performance of detecting samples from a specific generative model is evaluated on its synthetic images and the corresponding real images (balanced classes), which are RAISE-1K for *SynthBuster+*, CLIC for *SynthCLIC*, and model-specific sets for *CNNSpot*. We then calculate mAP over all generators and report the results in Table 3. We note that the performance on *CNNSpot* is 0.96 mAP and thus higher than reported by [39] (0.934 mAP) on the same test set. We also use linear probes, as done in [39], and show that there is only a small difference in performance, with the largest gap (+0.05) on *SynthBuster+* using *CNNSpot* as the training set.

Test Set	Training Set			
	CNNSpot	SynthBuster+	SynthCLIC	Combined
CNNSpot	0.96	0.67	0.37	0.84
SynthBuster+	0.66	0.99	0.79	0.96
SynthCLIC	0.56	0.64	0.92	0.87
CNNSpot (linear probe)	0.97	0.67	0.38	0.84
SynthBuster+ (linear probe)	0.61	0.99	0.78	0.96
SynthCLIC (linear probe)	0.52	0.64	0.92	0.88

**Table 3:** Mean AP for models trained on different training sets (columns) and evaluated on different test sets (rows). Combined refers to a model trained on the pooled training splits over all datasets. We also show results of linear probes.

Table 3 shows that cross-dataset results are significantly worse than in-dataset results, suggesting the datasets exhibit different characteristics. Consistent with this, the patterns observed in 2D projections of CLIP embeddings vary visibly, with clear separability of the classes on *CNNSpot* and much more entanglement for the diffusion-based datasets, see Appendix B.2 for figures.

## 4.2 Interpreting Linear Projections

We project CLIP image representations with  $\mathbf{W}_{\mathbf{L}1} \in \mathbb{R}^{d \times k}$  to  $k = 8$  dimensions and optimize for orthogonality in this layer’s activations (see Section 3.3). We confirm that the weights in this layer—the column vectors of  $\mathbf{W}_{\mathbf{L}1}$ —are roughly orthogonal. This suggests different aspects or concepts are extracted from the images to model the SID task.

We assess the importance of each column vector in  $\mathbf{W}_{\mathbf{L}1}$  following the approach described in Section 3.4 (see Figure 4). Across all models, column vector three  $\mathbf{W}_{\mathbf{L}1(:,3)}$  is the most relevant, followed by  $\mathbf{W}_{\mathbf{L}1(:,1)}$ . Particularly, for the model trained on *CNNSpot*,  $\mathbf{W}_{\mathbf{L}1(:,3)}$  is highly relevant. Visual inspection of the distribution over the activations of the projection of  $\mathbf{W}_{\mathbf{L}1(:,3)}$ , separated by class, shows that real and synthetic samples are nearly perfectly separated by just using this projection. Overall, this means  $k = 8$  is likely higher than necessary for this task. In additional experiments (Appendix B.4), we found that varying the projection dimension between  $k = 2$  and  $k = 16$  had minimal impact on mAP ( $\leq 0.03$  absolute). Interestingly, the model weights learned from the different training datasets are quite similar. We hypothesize this might be due to the identical random initialization of the layer weights. We visualize the similarities across models in Appendix B.4.

		Logit Contributions (Synthetic - Real)							
		0.000	0.305	0.000	1.961	-0.009	0.056	0.078	0.184
Training Set	CNNSpot -	-0.018	0.429	0.007	1.457	0.066	0.058	0.138	0.017
	SynthCLIC -	0.102	0.825	-0.116	1.512	-0.134	0.025	0.235	0.296
	SynthBuster+ -	-0.045	0.721	-0.047	0.152	-0.037	0.088	0.066	0.963
	Combined -								

**Figure 4:** Shown are the difference in the mean contribution of each column of  $\mathbf{A}_{\mathbf{L}1}$  to the output logits between samples of the real and the synthetic class. High absolute values indicate strong contribution to class logits.

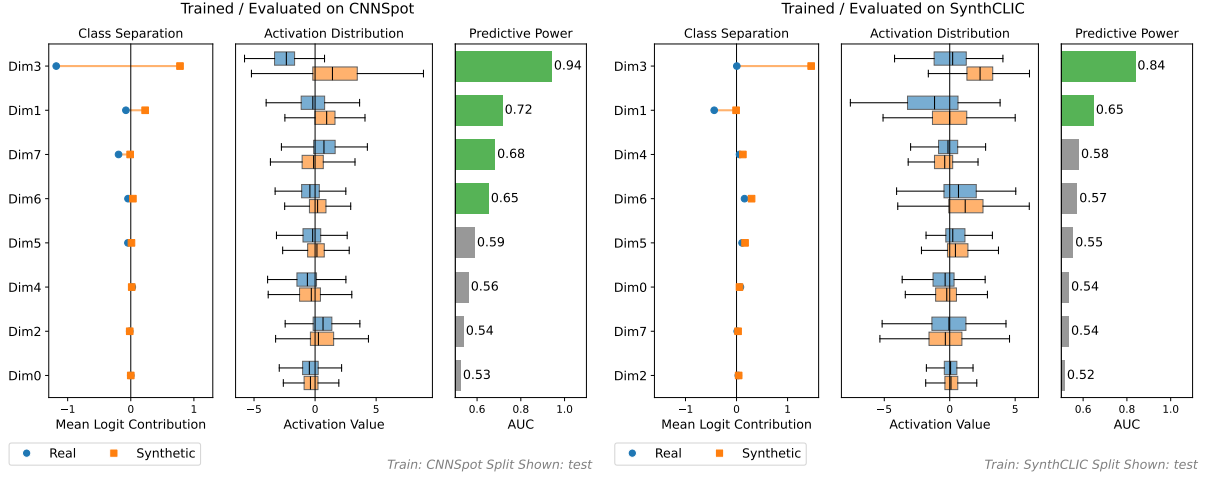


**Figure 5:** For each column vector in  $\mathbf{W}_{\mathbf{L}1}$  the following figures are shown (left panel for *CNNSpot*, right panel for *SynthCLIC*): Class separation shows the mean logit contribution for real (blue) and synthetic images (orange). Activation distribution shows boxplots of the activations in  $\mathbf{A}_{\mathbf{L}1}$  for real (blue) and synthetic images (orange). Predictive power shows AUC values for binary classifiers using the values of  $\mathbf{A}_{\mathbf{L}1}$ .

Figure 6 show the training set samples from *CNNSpot* and *SynthCLIC* with the highest and lowest activations for the most important projections  $\mathbf{W}_{\mathbf{L}1(:,3)}$  and  $\mathbf{W}_{\mathbf{L}1(:,1)}$  in  $\mathbf{A}_{\mathbf{L}1}$ —as indicated by their average logit contributions.

For the model trained on *CNNSpot* the samples with the highest activations along  $\mathbf{W}_{\mathbf{L}1(:,3)}$  show clear artifacts and are barely interpretable, while the samples with the lowest activations are clear and sharp. The samples along  $\mathbf{W}_{\mathbf{L}1(:,1)}$  are less directly relatable to SID—there are images of buses with high values and a mix of subjects with low values.

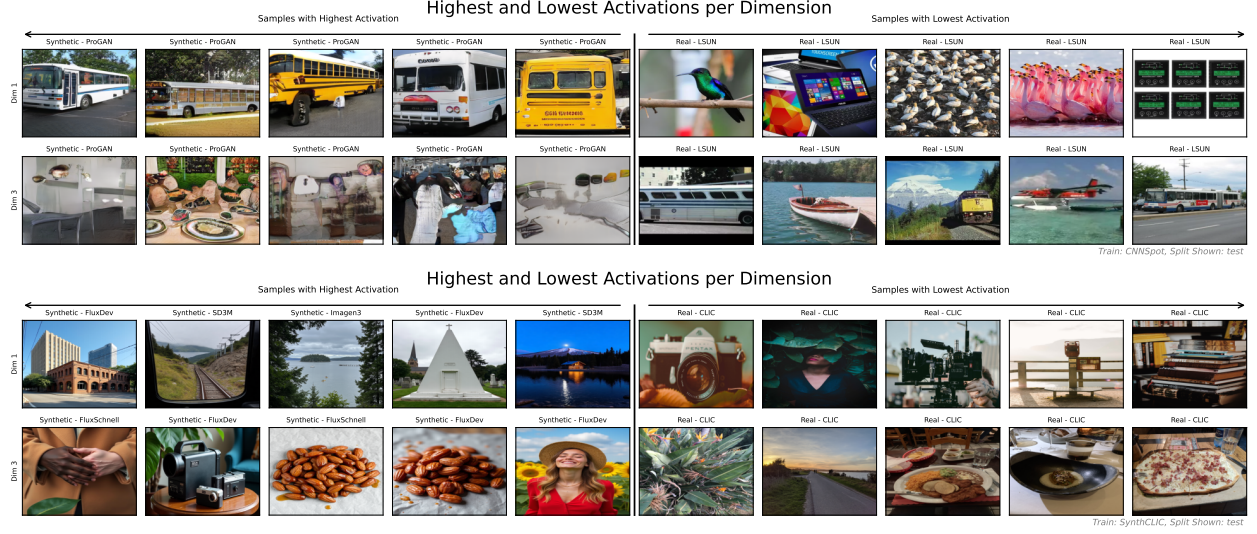


**Figure 6:** Images from CNNSpot (top) and SynthCLIC (bottom) with highest (first five images in each row, from the left) and lowest (images six through ten in each row, from left to right) activations per dimension (one row per dimension).

For SynthCLIC, visual interpretation of the top (all synthetic) and lowest (all real) scoring images along  $\mathbf{W}_{L1(:,1)}$  and  $\mathbf{W}_{L1(:,3)}$  is difficult. The projection defined by  $\mathbf{W}_{L1(:,3)}$  seems more clearly interpretable with the top scoring images having high saturation, while the lowest scoring images seem unprofessional with low contrast and sensor noise.

We interpret the learned projections following the approach described in Section 3.5 and rank terms from different vocabularies according to their similarities to the projections. Table 4 shows the terms with the highest similarity to the projected vectors  $\mathbf{W}_{L1(:,3)}$  and  $\mathbf{W}_{L1(:,1)}$  for CNNSpot. These seem indicative of the observed appearance, such as *Artwork with glitch art aesthetics* or *glitch-artifacts*. This indicates the model is able to detect clear visual artifacts. Projection  $\mathbf{W}_{L1(:,1)}$ , which is slightly less important, is more difficult to interpret and features lower similarity values between the concepts and the projection.

CNNSpot - Match to $\mathbf{W}_{L1(:,1)}$		
Rank	Antonyms	TextSpan
1	posterization (-0.155)	Collage of vintage magazine clippings (0.053)
2	lens-dirt (-0.129)	weathered religious icon (0.046)
3	desaturation (-0.117)	Stark and minimalist urban scene (0.041)
4	clarity (-0.116)	A chair (0.040)
5	halo-artifacts (-0.115)	Minimalist architectural photography (0.039)
CNNSpot - Match to $\mathbf{W}_{L1(:,3)}$		
Rank	Antonyms	TextSpan
1	depth-layering (-0.268)	Artwork with glitch art aesthetics (0.145)
2	fake-lens-effects (-0.244)	A digital glitch design (0.144)
3	glitch-artifacts (-0.238)	Ethereal double exposure photography (0.144)
4	print-texture (-0.220)	Detailed illustration of a futuristic bioreactor (0.137)
5	posterization (-0.214)	Artwork featuring digital glitch patterns (0.136)

**Table 4:** Shown are the vocabulary terms with the highest absolute (for Antonyms) and highest (for TextSpan) similarity to the learned model weights for a model trained on the CNNSpot dataset. For each term, the cosine similarity is shown in parentheses.

Table 5 shows the results for SynthCLIC. For projection  $\mathbf{W}_{L1(:,3)}$  terms involving variations of *minimalist* are the most similar. For  $\mathbf{W}_{L1(:,1)}$  the interpretation is less clear with significantly lower similarities for both vocabularies as compared to  $\mathbf{W}_{L1(:,3)}$ .

### 4.3 Concept Model

Table 6 shows the test results for different training sets. Mean AP is high when training and test set are from the same dataset, otherwise performance is substantially lower. When compared to our supervised baseline (Table 3),

SynthCLIC - Match to $W_{L1}(:,1)$		
Rank	Antonyms	TextSpan
1	cross-processing (0.146)	Majestic mountain (0.074)
2	specular-highlights (0.124)	A volcano (0.072)
3	composition-balance (0.121)	serene mountain scenery (0.069)
4	depth-layering (0.120)	Majestic mountain vista (0.066)
5	low-light-noise (0.119)	contemplative mountain view (0.062)
SynthCLIC - Match to $W_{L1}(:,3)$		
Rank	Antonyms	TextSpan
1	minimalist-style (0.244)	Minimalist white backdrop (0.170)
2	framing (0.229)	Minimalist lines (0.149)
3	depth-layering (0.219)	Stark minimalism (0.148)
4	instant-camera-cues (-0.217)	Photograph with the artistic style of minimalism (0.144)
5	panning (0.206)	Minimalist urban geometry (0.137)

**Table 5:** Shown are the vocabulary terms with the highest absolute (for Antonyms) and highest (for TextSpan) similarity to the learned model weights for a model trained on the SynthCLIC dataset. For each term, the cosine similarity is shown in parentheses. We rank by absolute similarity for  $C_{\text{antonyms}}$  but report the signed similarity; the sign indicates alignment with the (positive–negative) attribute direction.

performances are competitive overall, with a modest drop on *SynthCLIC* (0.04 – 0.07 mAP). The performance between the two vocabularies is similar with neither consistently outperforming the other.

Test Set	Vocabulary	Training Set			
		CNNSpot	SynthBuster+	SynthCLIC	Combined
CNNSpot	Antonyms	0.96	0.62	0.47	0.90
	TextSpan	0.96	0.64	0.40	0.89
SynthBuster+	Antonyms	0.53	0.99	0.79	0.99
	TextSpan	0.51	0.99	0.78	0.99
SynthCLIC	Antonyms	0.54	0.48	0.85	0.87
	TextSpan	0.53	0.53	0.88	0.88

**Table 6:** Mean Average Precision of different concept bottleneck models trained with different concept sets (Vocabulary) and training sets (columns), as evaluated on different test sets (rows).

Figure 1 shows one photograph and its corresponding synthetic variants from *SynthCLIC*. Visually, the synthetic examples appear of high quality, however, have a distinct look when compared to the real photograph. The real photograph has a lower contrast, less saturation and mild noise and grain, as well as a low level of detail. The synthetic photographs appear more professional with a similar, warm color palette and sharp details, as well as a shallow depth of field—particularly the variant from SD3M.

We inspect several metrics to assess concept importance for real and synthetic images on *SynthCLIC* and *CNNSpot* (see Figure 7). For both models, trained on *CNNSpot* and *SynthCLIC*, there are clear differences between the classes with respect to which concepts are selected. For *CNNSpot* the concepts with the highest activation probability and class separation identify synthetic images. The concepts indicate the presence of strong artifacts, such as *moire patterns* or *tiling artifacts*. For *SynthCLIC* the most relevant concepts are less discriminative as indicated by smaller gaps in the class separation panel. Some concepts seem (if selected) indicative for the synthetic class (*ringing artifacts* or *eye catchlight*). A number of concepts has near zero activation probability for synthetic images, however, low positive values (0.1) for real images, and contribute negatively to the logits (i.e. predict the real class). These are concepts, such as *glitch artifacts*, *scan artifacts*, *print texture*, or *object boundaries*.

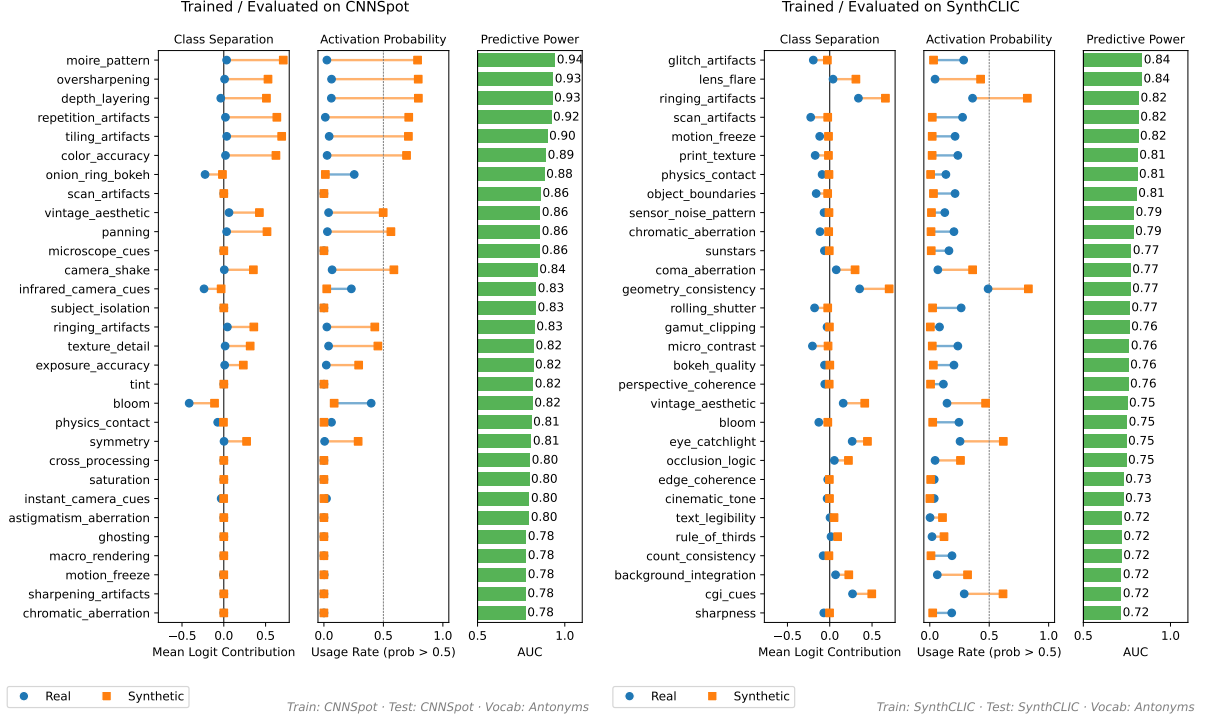


**Figure 7:** Shown are the top 30 concepts (according to predictive power) for a model trained and evaluated on *CNNSpot* (left) and *SynthCLIC* (right). For each dataset shown are (from left to right): Class Separation, defined as the mean logit contribution of each concepts for real (blue) and synthetic (orange) images, Activation Probability, defined as the fraction of images (for each class) concepts are activated (used) with at least 0.5 probability, Predictive Power, defined as single-feature (concept) AUC if it were used for a binary classifier. The concepts are from  $C_{\text{antonyms}}$ .

## 5 Discussion & Conclusion

We revisit the three research questions formulated in Section 1.

**Q1: How well do CLIP-based detectors scale from GAN-based to modern diffusion-based images, and how do they generalize across datasets?** Our experiments show that CLIP-based detectors perform extremely well on GAN-based images from *CNNSpot*, reaching near-perfect mAP in both in-dataset and cross-split evaluations. In contrast, performance drops on the diffusion-based *SynthBuster+* and *SynthCLIC* datasets, even though all models use the same frozen CLIP backbone. Cross-dataset evaluations further reveal that detectors trained on *CNNSpot* generalize poorly to *SynthBuster+* and *SynthCLIC*, and vice versa, while pooled training on multiple datasets improves but does not fully close the gap. These results indicate that CLIP does not provide a “universal” SID representation: the discriminative structure in CLIP space depends strongly on both the real-image distribution and the family of generative models seen during training.

**Q2: Can CLIP-based SID decisions be expressed as sparse combinations of human-interpretable concepts?** By adapting sparse linear concept discovery models to our SID setting, we find that concept bottlenecks can express decisions using a small number of photography- and forensics-oriented concepts while remaining competitive with standard linear heads. Across datasets, this interpretability comes with a modest performance cost, most notably on the more challenging *SynthCLIC* setting. The selected concepts are intuitive and often correspond to recognizable cues (e.g., *moire pattern*, *ringing artifacts*, *lens flare*), providing a compact explanation of why an image is classified as real or synthetic. At the same time, concept models are more sensitive than simple linear heads to the choice of vocabulary and sparsity hyperparameters, making vocabulary construction a non-trivial design choice in practice.

**Q3: Which aspects of an image does CLIP actually use for synthetic image detection?** Our analyses suggest that CLIP-based detectors rely primarily on high-level photographic and semantic cues rather than stable, model-specific fingerprints. The orthogonal linear head on CLIP’s last hidden state reveals directions that contribute positively or

negatively to the synthetic class. Images that strongly activate these directions exhibit characteristic photographic traits such as *minimalist style*, *framing*, or *cross-processing*. In addition, CLIP-IQA attributes show systematic shifts between real and synthetic images in perceived *quality*, *noisiness*, and *sharpness*. On older GAN-based data, these cues often coincide with visible artifacts and compositional issues, whereas on high-quality diffusion images they manifest as more subtle stylistic and aesthetic differences. Overall, CLIP-based SID appears to exploit how images *look and feel* as photographs, rather than relying on explicit generator fingerprints.

**Limitations and future work.** Our study is limited to a single CLIP backbone and to three datasets with photographic images and a finite set of generative models. As a result, our conclusions may not fully transfer to non-photographic domains (e.g., medical or scientific imaging) or to future generators with qualitatively different failure modes. Moreover, our analysis focuses on semantic and photographic cues and does not explicitly combine them with low-level fingerprint-based features or cryptographic watermarking. Future work should explore hybrid detectors that jointly exploit semantic CLIP embeddings and forensic cues, extend our analysis to additional backbones and modalities, and investigate continual or online adaptation as new generators appear.

In summary, our results show that CLIP-based methods are powerful but not universal tools for synthetic image detection. They excel on older GAN-based content, struggle more with high-quality diffusion images and cross-dataset generalization, and primarily rely on high-level photographic attributes rather than explicit generator fingerprints. Sparse concept bottlenecks offer a promising way to expose and control these cues, but they require careful vocabulary design and regularization. We hope that our datasets, models, and analyses provide a useful basis for developing more robust and interpretable SID systems that can keep pace with rapidly evolving generative models.

## 6 Data & Code Availability

We will release *SynthCLIC*, *SynthBuster+*, the images used in *CNNSpot*, our vocabulary  $C_{\text{antonyms}}$ , the prompts for *SynthCLIC* and *SynthBuster+*, the model checkpoints, and all inference code upon publication<sup>3</sup>, subject to the licenses of the underlying photographs.

## References

- [1] *Adobe Firefly*. URL: <https://www.adobe.com/products/firefly.html>.
- [2] *Announcing Black Forest Labs*. Jan. 2024. URL: <https://bfl.ai/announcements/24-08-01-bfl> (visited on 05/13/2025).
- [3] Quentin Bammey. “Synthbuster: Towards Detection of Diffusion Model Generated Images”. In: *IEEE Open Journal of Signal Processing* (2023), pp. 1–9. ISSN: 2644-1322. DOI: 10.1109/OJSP.2023.3337714. URL: <https://ieeexplore.ieee.org/document/10334046/> (visited on 03/11/2024).
- [4] Nicholas Carlini and Hany Farid. “Evading Deepfake-Image Detectors with White- and Black-Box Attacks”. In: *2020 IEEE/CVF Conference on Computer Vision and Pattern Recognition Workshops (CVPRW)*. Seattle, WA, USA: IEEE, June 2020, pp. 2804–2813. ISBN: 978-1-72819-360-1. DOI: 10.1109/CVPRW50498.2020.00337. URL: <https://ieeexplore.ieee.org/document/9150604/> (visited on 03/14/2024).
- [5] Mirko Casu et al. *AI Mirage: The Impostor Bias and the Deepfake Detection Challenge in the Era of Artificial Illusions*. arXiv:2312.16220 [cs]. Dec. 2023. URL: <http://arxiv.org/abs/2312.16220> (visited on 02/28/2024).
- [6] Mehdi Cherti et al. “Reproducible scaling laws for contrastive language-image learning”. In: *2023 IEEE/CVF Conference on Computer Vision and Pattern Recognition (CVPR)*. arXiv:2212.07143 [cs]. June 2023, pp. 2818–2829. DOI: 10.1109/CVPR52729.2023.00276. URL: <http://arxiv.org/abs/2212.07143> (visited on 05/13/2025).
- [7] Bobby Chesney and Danielle Citron. “Deep fakes: A looming challenge for privacy, democracy, and national security”. In: *Calif. L. Rev.* 107 (2019), p. 1753. DOI: <https://dx.doi.org/10.2139/ssrn.3213954>.
- [8] Dario Cioni et al. *Are CLIP features all you need for Universal Synthetic Image Origin Attribution?* arXiv:2408.09153 [cs]. Aug. 2024. URL: <http://arxiv.org/abs/2408.09153> (visited on 10/08/2024).
- [9] Gheorghe Comanici et al. *Gemini 2.5: Pushing the Frontier with Advanced Reasoning, Multimodality, Long Context, and Next Generation Agentic Capabilities*. arXiv:2507.06261 [cs]. Oct. 2025. DOI: 10.48550/arXiv.2507.06261. URL: <http://arxiv.org/abs/2507.06261> (visited on 12/03/2025).

<sup>3</sup><https://github.com/marco-willi/clip-cues>

[10] Sean Cordey. *Cyber Influence Operations: An Overview and Comparative Analysis*. en. Tech. rep. Artwork Size: 38 p. Medium: application/pdf. ETH Zurich, Oct. 2019, 38 p. DOI: 10.3929/ETHZ-B-000382358. URL: <http://hdl.handle.net/20.500.11850/382358> (visited on 06/16/2023).

[11] Riccardo Corvi et al. “Intriguing properties of synthetic images: from generative adversarial networks to diffusion models”. In: *2023 IEEE/CVF Conference on Computer Vision and Pattern Recognition Workshops (CVPRW)*. Vancouver, BC, Canada: IEEE, June 2023, pp. 973–982. ISBN: 9798350302493. DOI: 10.1109/CVPRW59228.2023.00104. URL: <https://ieeexplore.ieee.org/document/10209003/> (visited on 03/05/2024).

[12] Riccardo Corvi et al. “On The Detection of Synthetic Images Generated by Diffusion Models”. In: *ICASSP 2023 - 2023 IEEE International Conference on Acoustics, Speech and Signal Processing (ICASSP)*. Rhodes Island, Greece: IEEE, June 2023, pp. 1–5. ISBN: 978-1-72816-327-7. DOI: 10.1109/ICASSP49357.2023.10095167. URL: <https://ieeexplore.ieee.org/document/10095167/> (visited on 03/05/2024).

[13] Davide Cozzolino et al. *ForensicTransfer: Weakly-supervised Domain Adaptation for Forgery Detection*. arXiv:1812.02510 [cs]. Nov. 2019. URL: <http://arxiv.org/abs/1812.02510> (visited on 03/14/2024).

[14] Davide Cozzolino et al. “Raising the bar of ai-generated image detection with clip”. In: *Proceedings of the IEEE/CVF Conference on Computer Vision and Pattern Recognition*. 2024, pp. 4356–4366.

[15] Davide Cozzolino et al. “Zero-Shot Detection of AI-Generated Images”. en. In: *Computer Vision – ECCV 2024*. Ed. by Aleš Leonardis et al. Vol. 15076. Series Title: Lecture Notes in Computer Science. Cham: Springer Nature Switzerland, 2025, pp. 54–72. ISBN: 978-3-031-72649-1. DOI: 10.1007/978-3-031-72649-1\_4. URL: [https://link.springer.com/10.1007/978-3-031-72649-1\\_4](https://link.springer.com/10.1007/978-3-031-72649-1_4) (visited on 02/12/2025).

[16] Duc-Tien Dang-Nguyen et al. “RAISE: a raw images dataset for digital image forensics”. en. In: *Proceedings of the 6th ACM Multimedia Systems Conference*. Portland Oregon: ACM, Mar. 2015, pp. 219–224. ISBN: 978-1-4503-3351-1. DOI: 10.1145/2713168.2713194. URL: <https://dl.acm.org/doi/10.1145/2713168.2713194> (visited on 11/13/2024).

[17] Vincenzo De Rosa et al. “Exploring the Adversarial Robustness of CLIP for AI-generated Image Detection”. In: *2024 IEEE International Workshop on Information Forensics and Security (WIFS)*. Rome, Italy: IEEE, Dec. 2024, pp. 1–6. ISBN: 9798350364422. DOI: 10.1109/WIFS61860.2024.10810719. URL: <https://ieeexplore.ieee.org/document/10810719/> (visited on 02/12/2025).

[18] Laurent Dinh, Jascha Sohl-Dickstein, and Samy Bengio. *Density estimation using Real NVP*. arXiv:1605.08803 [cs]. Feb. 2017. DOI: 10.48550/arXiv.1605.08803. URL: <http://arxiv.org/abs/1605.08803> (visited on 05/13/2025).

[19] Alexey Dosovitskiy et al. “An Image is Worth 16x16 Words: Transformers for Image Recognition at Scale”. In: *arXiv:2010.11929 [cs]* (Oct. 2020). arXiv: 2010.11929. URL: <http://arxiv.org/abs/2010.11929> (visited on 05/18/2021).

[20] David C. Epstein et al. “Online Detection of AI-Generated Images”. In: *2023 IEEE/CVF International Conference on Computer Vision Workshops (ICCVW)*. Paris, France: IEEE, Oct. 2023, pp. 382–392. DOI: 10.1109/ICCVW60793.2023.00045. URL: <https://ieeexplore.ieee.org/document/10350523/> (visited on 03/04/2024).

[21] Patrick Esser et al. *Scaling Rectified Flow Transformers for High-Resolution Image Synthesis*. arXiv:2403.03206 [cs]. Mar. 2024. DOI: 10.48550/arXiv.2403.03206. URL: <http://arxiv.org/abs/2403.03206> (visited on 05/13/2025).

[22] Hany Farid. “Creating, Using, Misusing, and Detecting Deep Fakes”. In: *Journal of Online Trust and Safety* 1.4 (Sept. 2022). ISSN: 2770-3142. DOI: 10.54501/jots.v1i4.56. URL: <https://tsjournal.org/index.php/jots/article/view/56> (visited on 03/07/2024).

[23] Tatiana Gaintseva et al. *Improving Interpretability and Robustness for the Detection of AI-Generated Images*. arXiv:2406.15035 [cs]. June 2024. URL: <http://arxiv.org/abs/2406.15035> (visited on 08/12/2024).

[24] Yossi Gandelsman, Alexei A. Efros, and Jacob Steinhardt. *Interpreting CLIP’s Image Representation via Text-Based Decomposition*. arXiv:2310.05916 [cs]. Mar. 2024. DOI: 10.48550/arXiv.2310.05916. URL: <http://arxiv.org/abs/2310.05916> (visited on 03/18/2025).

[25] Ian J. Goodfellow et al. “Generative adversarial nets”. In: *Advances in Neural Information Processing Systems* 3. January (2014), pp. 2672–2680. ISSN: 10495258. DOI: 10.3156/jsoft.29.5\_177\_2.

[26] Jonathan Ho, Ajay Jain, and Pieter Abbeel. *Denoising Diffusion Probabilistic Models*. arXiv:2006.11239 [cs]. Dec. 2020. DOI: 10.48550/arXiv.2006.11239. URL: <http://arxiv.org/abs/2006.11239> (visited on 05/13/2025).

[27] Jinbin Huang et al. *ASAP: Interpretable Analysis and Summarization of AI-generated Image Patterns at Scale*. arXiv:2404.02990 [cs]. Apr. 2024. URL: <http://arxiv.org/abs/2404.02990> (visited on 08/12/2024).

[28] Imagen-Team-Google et al. *Imagen 3*. arXiv:2408.07009 [cs]. Dec. 2024. DOI: 10.48550/arXiv.2408.07009. URL: <http://arxiv.org/abs/2408.07009> (visited on 05/13/2025).

[29] *Introducing 4o Image Generation*. Mar. 2025. URL: <https://openai.com/index/introducing-4o-image-generation/> (visited on 05/13/2025).

[30] Sohail Ahmed Khan and Duc-Tien Dang-Nguyen. *CLIPping the Deception: Adapting Vision-Language Models for Universal Deepfake Detection*. arXiv:2402.12927 [cs]. Feb. 2024. DOI: <https://doi.org/10.48550/arXiv.2402.12927>. URL: <http://arxiv.org/abs/2402.12927> (visited on 03/13/2024).

[31] Diederik P. Kingma and Max Welling. “Auto-Encoding Variational Bayes”. In: *CoRR* abs/1312.6114 (2013). URL: <https://api.semanticscholar.org/CorpusID:216078090>.

[32] Christos Koutlis and Symeon Papadopoulos. *Leveraging Representations from Intermediate Encoder-blocks for Synthetic Image Detection*. arXiv:2402.19091 [cs]. Feb. 2024. DOI: <https://doi.org/10.48550/arXiv.2402.19091>. URL: <http://arxiv.org/abs/2402.19091> (visited on 03/13/2024).

[33] Yaron Lipman et al. *Flow Matching for Generative Modeling*. arXiv:2210.02747 [cs]. Feb. 2023. DOI: 10.48550/arXiv.2210.02747. URL: <http://arxiv.org/abs/2210.02747> (visited on 05/13/2025).

[34] Zeyu Lu et al. *Seeing is not always believing: Benchmarking Human and Model Perception of AI-Generated Images*. arXiv:2304.13023 [cs]. Sept. 2023. URL: <http://arxiv.org/abs/2304.13023> (visited on 03/07/2024).

[35] Laurens van der Maaten and Geoffrey E. Hinton. “Visualizing Data using t-SNE”. In: *Journal of Machine Learning Research* 9 (2008), pp. 2579–2605. URL: <https://api.semanticscholar.org/CorpusID:5855042>.

[36] Francesco Marra et al. “Do GANs Leave Artificial Fingerprints?” In: *2019 IEEE Conference on Multimedia Information Processing and Retrieval (MIPR)*. San Jose, CA, USA: IEEE, Mar. 2019, pp. 506–511. ISBN: 978-1-72811-198-8. DOI: 10.1109/MIPR.2019.00103. URL: <https://ieeexplore.ieee.org/document/8695364/> (visited on 03/05/2024).

[37] *Midjourney*. URL: <https://www.midjourney.com/home/>.

[38] Sophie J. Nightingale and Hany Farid. “AI-synthesized faces are indistinguishable from real faces and more trustworthy”. en. In: *Proceedings of the National Academy of Sciences* 119.8 (Feb. 2022), e2120481119. ISSN: 0027-8424, 1091-6490. DOI: 10.1073/pnas.2120481119. URL: <https://pnas.org/doi/full/10.1073/pnas.2120481119> (visited on 03/07/2024).

[39] Utkarsh Ojha, Yuheng Li, and Yong Jae Lee. “Towards Universal Fake Image Detectors That Generalize Across Generative Models”. In: *Proceedings of the IEEE/CVF Conference on Computer Vision and Pattern Recognition (CVPR)*. June 2023, pp. 24480–24489. URL: [arxiv.org/pdf/2302.10174](http://arxiv.org/pdf/2302.10174).

[40] Aaron van den Oord, Nal Kalchbrenner, and Koray Kavukcuoglu. *Pixel Recurrent Neural Networks*. arXiv:1601.06759 [cs]. Aug. 2016. DOI: 10.48550/arXiv.1601.06759. URL: <http://arxiv.org/abs/1601.06759> (visited on 05/13/2025).

[41] Konstantinos P. Panousis, Dino Ienco, and Diego Marcos. *Sparse Linear Concept Discovery Models*. arXiv:2308.10782 [cs]. Aug. 2023. DOI: 10.48550/arXiv.2308.10782. URL: <http://arxiv.org/abs/2308.10782> (visited on 04/02/2025).

[42] Dustin Podell et al. *SDXL: Improving Latent Diffusion Models for High-Resolution Image Synthesis*. arXiv:2307.01952 [cs]. July 2023. URL: <http://arxiv.org/abs/2307.01952> (visited on 08/03/2023).

[43] Alec Radford et al. “Learning Transferable Visual Models From Natural Language Supervision”. In: *Proceedings of the 38th International Conference on Machine Learning*. Ed. by Marina Meila and Tong Zhang. Vol. 139. Proceedings of Machine Learning Research. PMLR, July 2021, pp. 8748–8763. URL: <https://proceedings.mlr.press/v139/radford21a.html>.

[44] Jonas Ricker et al. *Towards the Detection of Diffusion Model Deepfakes*. arXiv:2210.14571 [cs]. Jan. 2024. URL: <http://arxiv.org/abs/2210.14571> (visited on 03/05/2024).

[45] Robin Rombach et al. *High-Resolution Image Synthesis with Latent Diffusion Models*. arXiv:2112.10752 [cs]. Apr. 2022. URL: <http://arxiv.org/abs/2112.10752> (visited on 01/16/2023).

[46] Christoph Schuhmann et al. *LAION-5B: An open large-scale dataset for training next generation image-text models*. arXiv:2210.08402 [cs]. Oct. 2022. DOI: 10.48550/arXiv.2210.08402. URL: <http://arxiv.org/abs/2210.08402> (visited on 05/13/2025).

[47] Zeyang Sha et al. *DE-FAKE: Detection and Attribution of Fake Images Generated by Text-to-Image Generation Models*. arXiv:2210.06998 [cs]. Jan. 2023. URL: <http://arxiv.org/abs/2210.06998> (visited on 03/05/2024).

[48] Diangarti Tariang et al. *Synthetic Image Verification in the Era of Generative AI: What Works and What Isn't There Yet*. arXiv:2405.00196 [cs]. Apr. 2024. DOI: 10.48550/arXiv.2405.00196. URL: <http://arxiv.org/abs/2405.00196> (visited on 02/12/2025).

[49] Jianyi Wang, Kelvin C. K. Chan, and Chen Change Loy. *Exploring CLIP for Assessing the Look and Feel of Images*. arXiv:2207.12396 [cs]. Nov. 2022. DOI: 10.48550/arXiv.2207.12396. URL: <http://arxiv.org/abs/2207.12396> (visited on 03/07/2025).

[50] Sheng-Yu Wang et al. “CNN-generated images are surprisingly easy to spot... for now”. In: *Proceedings of the IEEE/CVF conference on computer vision and pattern recognition*. 2020, pp. 8695–8704. URL: <http://arxiv.org/abs/1912.11035>.

[51] Zhendong Wang et al. “DIRE for Diffusion-Generated Image Detection”. In: *2023 IEEE/CVF International Conference on Computer Vision (ICCV)*. Paris, France: IEEE, Oct. 2023, pp. 22388–22398. ISBN: 9798350307184. DOI: 10.1109/ICCV51070.2023.02051. URL: <https://ieeexplore.ieee.org/document/10377654/> (visited on 03/07/2024).

[52] Yung Jer Wong and Teck Khim Ng. *Local Statistics for Generative Image Detection*. arXiv:2310.16684 [cs]. Oct. 2023. URL: <http://arxiv.org/abs/2310.16684> (visited on 03/05/2024).

[53] Haiwei Wu, Jiantao Zhou, and Shile Zhang. *Generalizable Synthetic Image Detection via Language-guided Contrastive Learning*. arXiv:2305.13800 [cs]. May 2023. URL: <http://arxiv.org/abs/2305.13800> (visited on 03/07/2024).

[54] Shukang Yin et al. “A Survey on Multimodal Large Language Models”. In: *National Science Review* 11.12 (Nov. 2024). arXiv:2306.13549 [cs], nwae403. ISSN: 2095-5138, 2053-714X. DOI: 10.1093/nsr/nwae403. URL: <http://arxiv.org/abs/2306.13549> (visited on 05/13/2025).

[55] Fisher Yu et al. *LSUN: Construction of a Large-scale Image Dataset using Deep Learning with Humans in the Loop*. arXiv:1506.03365 [cs]. June 2016. DOI: 10.48550/arXiv.1506.03365. URL: <http://arxiv.org/abs/1506.03365> (visited on 05/21/2025).

[56] Jiahui Yu et al. *Scaling Autoregressive Models for Content-Rich Text-to-Image Generation*. arXiv:2206.10789 [cs]. June 2022. DOI: 10.48550/arXiv.2206.10789. URL: <http://arxiv.org/abs/2206.10789> (visited on 05/13/2025).

[57] Xu Zhang, Svebor Karaman, and Shih-Fu Chang. “Detecting and Simulating Artifacts in GAN Fake Images”. In: *2019 IEEE International Workshop on Information Forensics and Security (WIFS)*. Delft, Netherlands: IEEE, Dec. 2019, pp. 1–6. ISBN: 978-1-72813-217-4. DOI: 10.1109/WIFS47025.2019.9035107. URL: <https://ieeexplore.ieee.org/document/9035107/> (visited on 07/17/2024).

[58] Chunting Zhou et al. *Transfusion: Predict the Next Token and Diffuse Images with One Multi-Modal Model*. arXiv:2408.11039 [cs]. Aug. 2024. DOI: 10.48550/arXiv.2408.11039. URL: <http://arxiv.org/abs/2408.11039> (visited on 05/02/2025).

[59] Ziyin Zhou et al. “StealthDiffusion: Towards Evading Diffusion Forensic Detection through Diffusion Model”. In: *ACM Multimedia 2024*. 2024. URL: <https://openreview.net/forum?id=jnQFcUU9Bw>.

## A Methodological Details

### A.1 Datasets - *CNNSpot* Samples

Figure 8 shows a few example images from the *CNNSpot* training set.

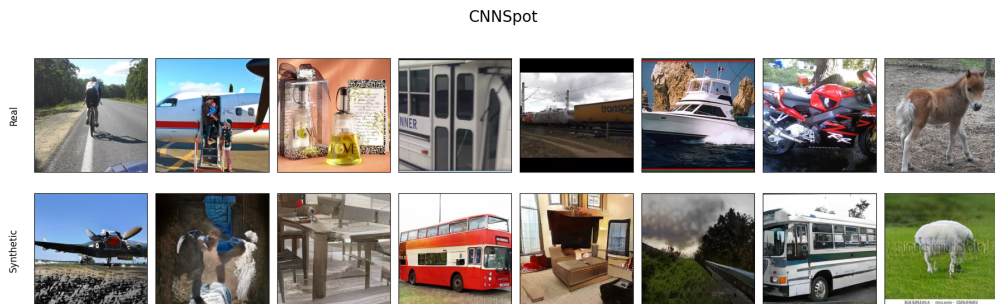


**Figure 8:** Examples from the *CNNSpot* training dataset. It consists of ProGAN generated synthetic images (bottom row) and images from different object categories of the LSUN dataset (top row).

## A.2 Datasets - Generative Models Used

For the datasets *SynthBuster+* and *SynthCLIC*, we generated synthetic images and captions using the following model versions: Imagen3 [28]<sup>4</sup>, FluxDev<sup>5</sup>, FluxSchnell<sup>6</sup>, Stable Diffusion 3 Medium<sup>7</sup>, and Gemini<sup>8</sup> (for caption generation).

## A.3 CLIP Classifier - Implementation Details

Table 7 lists the implementation details for the CLIP classifier model (see Section 3.3. Classes were imbalanced during model training, however, we did not apply special handling such as balancing / sampling or loss weighting. For this reason we use, as in other works, threshold independent metrics.

*Table 7: Implementation Details for CLIP Classifier*

Category	Parameter	Value	Notes
Training	Max Epochs	200	With early stopping
	Batch Size	64	
	Early Stopping Patience	5 epochs	Based on validation loss
	Validation Frequency	Every 1 epoch	
	Random Seed	123	All experiments
	Precision	b16-mixed	Mixed-precision training
	Accelerator	gpu (single)	
	Type	Adam	torch.optim.Adam
	Learning Rate	$1e - 3$ (default)	
	Weight Decay	0.01	
Optimizer	Beta Parameters	(0.9, 0.999)	defaults
	Epsilon	$1e - 8$	default
	Label Smoothing	0.1	Applied to BCE loss
	Orthogonality Loss Weight	0.33	
Data Aug. (Training)	RandomResizedCrop	scale=(0.5, 1.0), size=512	Crop 50-100% of original, resize to 512x512 (Augmentations are applied before CLIP preprocessing; the final input is resized to the model's resolution.)
Data Aug. (Val/Test)	RandomHorizontalFlip	p=0.5	50% probability
	RandomJPEGCompression	quality=(65, 100)	Uniform sampling
	RGB Conversion	Always applied	Ensures 3-channel format
	Augmentations	None	
Model Architecture	Preprocessing	Model-dependent	Normalization and resize openai/clip-vit-large-patch14-336
	Feature Extractor	clip-large-patch14	Final layer before classification
Loss Function	Feature Extraction Layer		No gradient updates to CLIP
	Frozen Backbone	Yes	Single hidden layer with 8 units
	Classification Head	orthogonal activation head	Binary classification logit
	Hidden Dimensions	8	Applied to weights
	Output Dimension	1	
	Activation Function	None (linear)	
	Orthogonal Initialization	Yes	
	Primary Loss	Binary Cross-Entropy with Logits	
	Label Smoothing	$y = y * (1 - \epsilon) + (1 - y) * \epsilon$	$\epsilon = 0.1$
	Auxiliary Losses	Orthogonality, Sparsity	

<sup>4</sup>[Imagen-3.0-generate-002](https://huggingface.co/Imagen3-0.0)

<sup>5</sup><https://huggingface.co/black-forest-labs/FLUX.1-dev>

<sup>6</sup><https://huggingface.co/black-forest-labs/FLUX.1-schnell>

<sup>7</sup><https://huggingface.co/stabilityai/stable-diffusion-3-medium>

<sup>8</sup>[gemini-2.0-flash-001](https://huggingface.co/gemini-2.0-flash-001)

#### A.4 Concept Model - Implementation Details

Table 8 shows the implementation details of the concept model (see Section 3.6).

**Table 8: Hyperparameters for Concept Bottleneck Model Experiments**

Category	Parameter	Value
Training	Max Epochs	4000
	Batch Size	256
	Early Stopping Patience	10 epochs
	Validation Frequency	Every 40 epochs
	Random Seed	123
Optimizer	Early Stopping Metric	val/loss
	Type	AdamW
	Learning Rate	$1 \times 10^{-3}$
Model	Weight Decay	$1 \times 10^{-4}$
	Temperature ( $\tau$ )	0.1
	Sparsity Weight ( $\beta$ )	$1 \times 10^{-4}$
Vocabularies	Target Sparsity ( $\alpha$ )	$1 \times 10^{-4}$
	Antonyms	168 concept pairs
	TextSpan	3,097 concepts

## B Additional Results

### B.1 Characterizing Datasets with CLIP-IQA

We use CLIP-IQA [49] to evaluate our datasets. The method compares image embeddings based on inputs without positional embeddings with contrastive textual descriptions of different attributes. Figure 9 shows the distributions across images generated from different sources.

### B.2 Analysing CLIP Image Embeddings with t-SNE

We use t-SNE [35] to reduce the dimensionality of CLIP image embeddings to visualize synthetic and real images in two dimensions, as done in [39, 30]. Figure 10 shows the results on the three datasets. While synthetic and real images from the *CNNSpot* dataset are well separated, with some semantic clustering (classes) visible, there is less clear separation for *SynthBuster+* and *SynthCLIC*, although, for both, the real data points are not evenly distributed—suggesting they can be separated to some degree by a classifier (e.g. a nearest neighbor classifier).

After training several models on different training sets, we use t-SNE to reduce the dimensionality of  $\mathbf{A}_{L1} \in \mathbb{R}^{n \times k}$  along the columns, where  $k = 8$ . The results show that the images of *CNNSpot* are separated well in all models, though best when the training set includes *CNNSpot* data. The visualizations in Figure 11 suggest that the data points of a given dataset are best separated when they are included in the training data.

### B.3 CLIP Zero-Shot Classification

We investigate how CLIP embeddings directly encode whether an image is AI generated or not. This was suggested [23], at least for GAN generated images. We create ten prompt pairs (for the positive and negative class) using ChatGPT and use them for CLIP zero-shot classification. A pair of example prompts are: *A real photograph* and *An AI-generated image*. The full set can be found in Table 11. We select the best performing prompt (mAP) as evaluated on each training split of a specific dataset and report the performance on the test splits of our datasets in Table 9. The only dataset with GAN-generated images, *CNNSpot*, achieves the highest mAP (0.81 - 0.82), regardless of the training set. *SynthCLIC* and *SynthBuster+* profit from prompt selection on their respective training split. This suggests zero-shot classification is sensitive to prompt selection and thus might not be practical in open-set scenarios without access to images from a generative model. Furthermore, mAP does not exceed 0.66 and 0.75, even with prompt selection. This indicates the prompts do not cover relevant aspects for the SID task. Results per model are shown in Table 10.

Table 10 shows the results per generative model. We calculate accuracy (ACC) by optimizing the decision threshold with respect to balanced accuracy (i.e. average recall) on each training set.

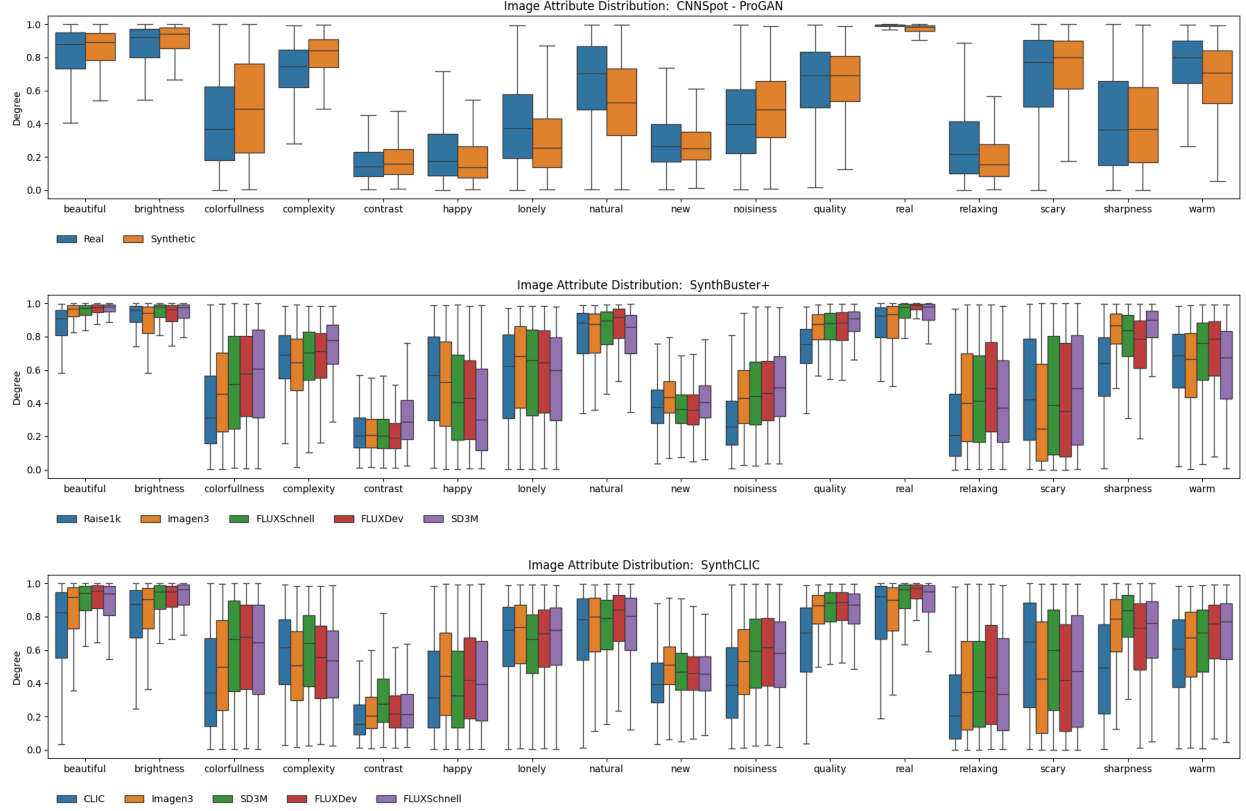


**Figure 9:** Image attributes scored with CLIP-IQA [49] are distributed differently across generative models and real images. Shown are results for CNNSpot (top, only training set), SynthBuster+ (middle), and SynthCLIC (bottom) and along different attributes (x-Axis) and their score (Y-Axis).

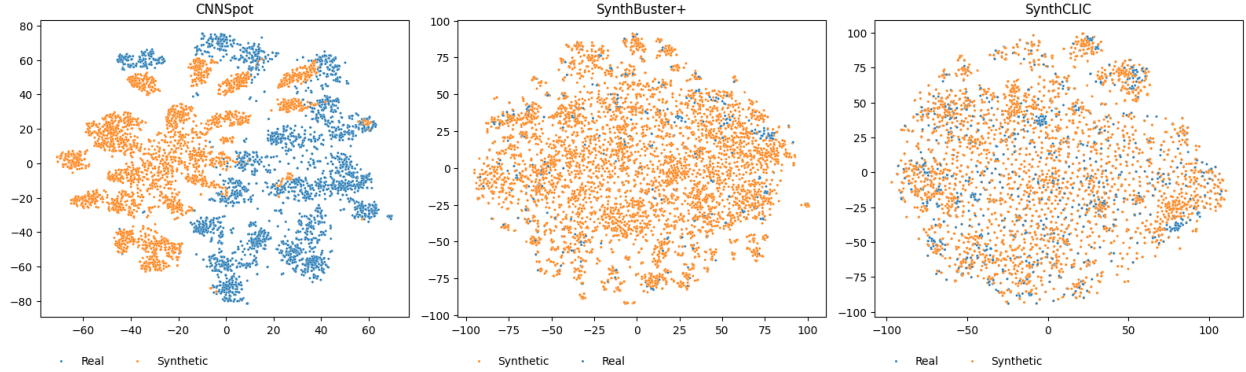


**Figure 10:** Dimensionality reduction with t-SNE shows clear separation of real (blue) and synthetic (orange) images for the GAN-based CNNSpot dataset, however, less so for SynthBuster+ and SynthCLIC.

The following text prompts (see Table 11) were used for CLIP zero-shot classification. Each set contains one prompt describing a real image and one describing a synthetic image. Prompt names are chosen to reflect their linguistic style or focus.

#### B.4 CLIP Classifier

Table 12 shows detailed results for each model.

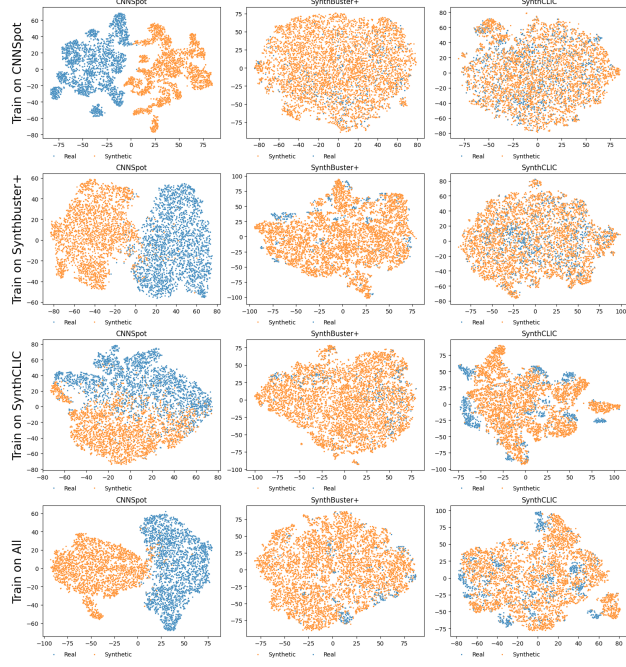


**Figure 11:** t-SNE of activations of data points from a distribution the model has seen during model training demonstrates more clear separation of real and synthetic data. Shown are different training datasets (rows) and test datasets (columns) and the corresponding distribution of real (blue) and synthetic (orange) images in a 2-D space.

Training Set (prompt selection)			
Test Set	CNNSpot	SynthBuster+	SynthCLIC
CNNSpot	0.81	0.82	0.82
SynthBuster+	0.64	0.75	0.69
SynthCLIC	0.47	0.57	0.66

**Table 9:** Mean Average Precision (mAP) for models trained (only prompt selection) on different training sets (columns) as evaluated on different test sets (rows).

Table 13 shows ablations with respect to the number  $k$  of orthogonal dimensions.

		Training Set					
		CNNSpot		SynthBuster+		SynthCLIC	
Test Sets		ACC	AP	ACC	AP	ACC	AP
CNNSpot	BigGAN	0.86	0.98	0.86	0.95	0.78	0.95
	CRN	0.90	0.99	0.60	0.94	0.77	0.86
	CycleGAN	0.88	1.00	0.76	0.95	0.65	0.87
	DALLE	0.64	0.80	0.75	0.83	0.75	0.84
	DeepFake	0.52	0.66	0.53	0.63	0.76	0.87
	GLIDE-100-10	0.53	0.54	0.67	0.72	0.65	0.69
	GLIDE-100-27	0.51	0.52	0.66	0.71	0.65	0.69
	GLIDE-50-27	0.52	0.53	0.64	0.68	0.65	0.69
	GauGAN	0.91	0.99	0.86	0.96	0.86	0.96
	Guided	0.63	0.74	0.61	0.71	0.65	0.71
	IMLE	0.79	0.98	0.58	0.91	0.78	0.93
	LDM-100	0.64	0.76	0.74	0.81	0.69	0.75
	LDM-200	0.63	0.75	0.74	0.81	0.69	0.76
	LDM-200-CFG	0.58	0.63	0.65	0.70	0.66	0.74
	ProGAN	0.84	0.99	0.82	0.92	0.66	0.82
	SAN	0.57	0.71	0.74	0.85	0.61	0.72
	SeeingDark	0.71	0.81	0.69	0.82	0.68	0.72
	StarGAN	0.84	0.98	0.72	0.79	0.61	0.95
	StyleGAN	0.77	0.90	0.79	0.86	0.68	0.88
	StyleGAN2	0.76	0.83	0.69	0.77	0.63	0.78
	WhichFacelsReal	0.91	0.98	0.90	0.97	0.87	0.98
SynthBuster+	DALLE2	0.58	0.61	0.60	0.65	0.55	0.57
	DALLE3	0.57	0.61	0.81	0.91	0.70	0.86
	Firefly	0.56	0.61	0.69	0.73	0.63	0.67
	FluxDev	0.56	0.58	0.66	0.70	0.62	0.68
	FluxSchnell	0.52	0.56	0.60	0.61	0.61	0.63
	Glide	0.72	0.81	0.77	0.88	0.67	0.73
	Imagen3	0.53	0.55	0.61	0.64	0.59	0.57
	MJv5	0.51	0.53	0.62	0.64	0.61	0.64
	SD1.3	0.60	0.65	0.73	0.81	0.63	0.70
	SD1.4	0.60	0.65	0.74	0.82	0.64	0.69
	SD2	0.68	0.78	0.75	0.86	0.61	0.68
	SD3M	0.59	0.63	0.67	0.71	0.64	0.72
	SDXL	0.65	0.74	0.73	0.81	0.70	0.77
SynthCLIC	FluxDev	0.45	0.45	0.54	0.56	0.62	0.65
	FluxSchnell	0.45	0.46	0.52	0.55	0.66	0.68
	Imagen3	0.46	0.46	0.53	0.55	0.56	0.59
	SD3M	0.49	0.49	0.58	0.61	0.66	0.71

**Table 10:** Results of zero-shot classification. Average precision (AP) and accuracy (ACC) for each combination of training set (columns) and test set (rows) including the specific generative models.

Prompt Set	Prompt
Generic	“A real photograph”
Neural network reference	“An AI-generated image”
Fake vs. real (camera emphasis)	“A real photograph”
Style and origin	“A neural network generated image”
Technical description	“A genuine photo taken with a camera”
Semantic truthfulness	“A fake image created by artificial intelligence”
Colloquial	“A natural photograph captured in the real world”
Colloquial (fake emphasis)	“A synthetic image generated by a machine learning model”
Conceptual framing	“An image captured by a physical camera sensor”
Artifact vs. capture	“An image produced by a generative model”
Semantic truthfulness	“An image representing a real-world scene”
Colloquial	“An image with no real-world counterpart”
Colloquial (fake emphasis)	“A real-life photo”
Conceptual framing	“An AI-made picture”
Artifact vs. capture	“A photo taken in the real world”
Semantic truthfulness	“A fake photo made by a computer”
Colloquial	“A real moment in time”
Colloquial (fake emphasis)	“An artificial creation”
Conceptual framing	“A true photographic capture”
Artifact vs. capture	“An unreal visual artifact”

**Table 11:** Prompt sets for CLIP zero-shot classification, covering a range of linguistic framings from technical to colloquial.

Training Set									
Test Sets	CNNSpot		SynthBuster+		SynthCLIC		Combined		
	ACC	AP	ACC	AP	ACC	AP	ACC	AP	
CNNSpot	BigGAN	0.97	1.00	0.52	0.83	0.36	0.36	0.82	0.96
	CRN	0.95	0.99	0.51	0.69	0.46	0.45	0.77	0.84
	CycleGAN	0.99	1.00	0.51	0.85	0.17	0.31	0.63	0.94
	DALLE	0.91	0.99	0.50	0.64	0.26	0.34	0.73	0.90
	DeepFake	0.67	0.92	0.50	0.57	0.47	0.47	0.64	0.78
	GLIDE-100-10	0.78	0.97	0.50	0.71	0.26	0.34	0.65	0.76
	GLIDE-100-27	0.78	0.97	0.50	0.70	0.26	0.34	0.63	0.73
	GLIDE-50-27	0.81	0.97	0.50	0.71	0.27	0.34	0.67	0.77
	GauGAN	1.00	1.00	0.54	0.93	0.35	0.33	0.86	0.99
	Guided	0.66	0.90	0.54	0.70	0.32	0.35	0.54	0.58
	IMLE	0.97	1.00	0.50	0.70	0.42	0.36	0.82	0.89
	LDM-100	0.96	1.00	0.50	0.72	0.17	0.32	0.73	0.88
	LDM-200	0.96	1.00	0.50	0.73	0.18	0.32	0.73	0.87
	LDM-200-CFG	0.79	0.96	0.50	0.65	0.38	0.39	0.70	0.81
	ProGAN	1.00	1.00	0.50	0.62	0.17	0.32	0.88	0.99
	SAN	0.50	0.73	0.52	0.66	0.50	0.51	0.48	0.52
	SeeingDark	0.75	0.87	0.55	0.87	0.40	0.40	0.66	0.78
	StarGAN	0.99	1.00	0.50	0.37	0.34	0.36	0.89	0.98
	StyleGAN	0.83	0.99	0.50	0.53	0.35	0.39	0.81	0.91
	StyleGAN2	0.70	0.99	0.50	0.47	0.43	0.45	0.76	0.84
	WhichFaceIsReal	0.96	1.00	0.52	0.52	0.46	0.44	0.69	0.94
SynthBuster+	DALLE2	0.56	0.83	0.87	0.96	0.42	0.46	0.72	0.85
	DALLE3	0.50	0.54	0.90	1.00	0.77	0.97	0.81	1.00
	Firefly	0.51	0.73	0.89	0.99	0.62	0.66	0.80	0.96
	FluxDev	0.50	0.37	0.90	1.00	0.76	0.97	0.80	0.97
	FluxSchnell	0.50	0.41	0.90	1.00	0.77	0.98	0.80	0.98
	Glide	0.59	0.90	0.90	1.00	0.57	0.62	0.76	0.89
	Imagen3	0.50	0.37	0.90	0.99	0.76	0.94	0.80	0.97
	MJV5	0.50	0.52	0.90	0.99	0.75	0.91	0.80	0.98
	SD1.3	0.55	0.78	0.90	1.00	0.63	0.74	0.80	0.98
	SD1.4	0.54	0.79	0.90	1.00	0.66	0.73	0.80	0.97
	SD2	0.69	0.91	0.90	1.00	0.48	0.55	0.79	0.97
	SD3M	0.50	0.62	0.90	1.00	0.75	0.94	0.81	0.98
	SDXL	0.58	0.84	0.90	1.00	0.62	0.74	0.80	0.99
SynthCLIC	FLUXDev	0.50	0.49	0.50	0.61	0.75	0.94	0.63	0.86
	FLUXSchnell	0.50	0.58	0.50	0.64	0.75	0.95	0.64	0.91
	Imagen3	0.50	0.47	0.50	0.59	0.74	0.88	0.63	0.82
	SD3M	0.51	0.69	0.50	0.70	0.75	0.92	0.64	0.89

**Table 12:** Test set evaluations of different generative models and models trained on different training sets. Shown are average precision (first) and accuracy (second).

Test Dataset	k	2	4	8	16
	CNNSpot	0.39	0.38	0.37	0.38
SynthBuster+	0.81	0.79	0.79	0.78	
SynthCLIC	0.91	0.94	0.92	0.92	

**Table 13:** Mean Average Precision (mAP) by dataset and k-value for models trained on SynthCLIC.